Silver Nanoparticle Aggregates as Highly Efficient Plasmonic Antennas for Fluorescence Enhancement

Ron Gill,*,[†] Lijin Tian,[‡] Walter R. C. Somerville,[§] Eric C. Le Ru,[§] Herbert van Amerongen,[‡,ǁ] and Vinod Subramaniam[†]

[†]Nanobiophysics Group, MIRA Institute for Biomedical Technology and Technical Medicine, University of Twente, PO Box 217, 7500 AE Enschede, The Netherlands
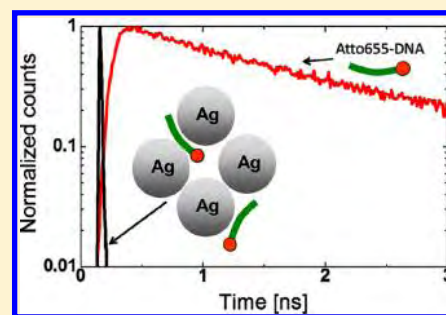
[‡]Laboratory of Biophysics, Wageningen University, P.O. Box 8128, 6700 ET, Wageningen, The Netherlands

[§]The MacDiarmid Institute for Advanced Materials and Nanotechnology, School of Chemical and Physical Sciences, Victoria University of Wellington, P.O. Box 600, Wellington 6140, New Zealand

[ǁ]MicroSpectroscopy Centre, Wageningen University, P.O. Box 8128, 6700 ET, Wageningen, The Netherlands

S *Supporting Information*

ABSTRACT: The enhanced local fields around plasmonic structures can lead to enhancement of the excitation and modification of the emission quantum yield of fluorophores. So far, high enhancement of fluorescence intensity from dye molecules was demonstrated using bow-tie gap antenna made by e-beam lithography. However, the high manufacturing cost and the fact that currently there are no effective ways to place fluorophores only at the gap prevent the use of these structures for enhancing fluorescence-based biochemical assays. We report on the simultaneous modification of fluorescence intensity and lifetime of dye-labeled DNA in the presence of aggregated silver nanoparticles. The nanoparticle aggregates act as efficient plasmonic antennas, leading to more than 2 orders of magnitude enhancement of the *average* fluorescence. This is comparable to the best-reported fluorescence enhancement for a single molecule but here applies to the average signal detected from all fluorophores in the system. This highlights the remarkable efficiency of this system for surface-enhanced fluorescence. Moreover, we show that the fluorescence intensity enhancement varies with the plasmon resonance position and measure a significant reduction (300×) of the fluorescence lifetime. Both observations are shown to be in agreement with the electromagnetic model of surface-enhanced fluorescence.

INTRODUCTION

Noble metal nanostructures, when illuminated close to their plasmon resonance, create enhanced local fields, leading to antenna-like behavior. These optical antennas,[1−3] similar to radio-frequency antennas in receiving mode, capture free-space electromagnetic radiation and focus it into a region that can be much smaller than the diffraction limit. Additionally, these nanoantennas can operate in transmission mode, enhancing and/or channeling the output of a nearby emitter into the far field.[4] Thus, there is a large interest in using these structures for the enhanced excitation and detection of fluorescence, so-called surface-enhanced fluorescence (SEF).[5] While even a single gold nanosphere can act as an optical antenna,[6,7] its efficiency in fluorescence enhancement is limited. The main reason for this limitation is that the plasmon resonance for spherical gold particles occurs in a wavelength range where losses (through optical absorption related to interband transitions) are important; i.e., the imaginary part of the dielectric function is relatively large. One possible solution to overcome this limitation is the use of different geometries and shapes, such as shells[8,9] or rods,[10,11] which shift the plasmon peak of the particle to a wavelength range with lower absorption losses,

leading to higher fluorescence enhancement. Alternatively, the use of silver instead of gold can lead to higher fluorescence enhancement,[12,13] as the plasmon resonance for silver spheres is at a wavelength where its optical absorption is low. To achieve even higher levels of fluorescence enhancement several groups have used gap-based antennas.[14−18] This type of antenna, where two or more metal structures are positioned with a small gap between them, can lead to much higher field enhancement than single particles, as most of the local field is confined to the gap.[19,20]

One possible application of plasmonic structures is to enhance the detection of dye-labeled molecules in biomolecular diagnostic assays. For this, the average enhancement of fluorescence over all dye molecules present (rather than the single molecule enhancement) is the important factor, and therefore discrete gap antennas made on surfaces by lithography are not effective because they concentrate the light to spots that are small and far apart. Interestingly, more

than 30 years ago, Creighton[21] published the first report of surface-enhanced Raman scattering (SERS) in aggregated noble metal colloids. Although it was many years before optical antennas were suggested, coaggregation of silver nanoparticles and the adsorbed target molecules form electromagnetic "hot-spots" in which very large surface-enhanced Raman signals are possible. Since then, these self-assembled gap-antenna-like superstructures have been heavily used for SERS,[22] including for the detection of Raman spectra of single molecules.[23−27]

We have recently shown that the "hot-spots" created in silver nanoparticle aggregates can also lead to very high enhancement of the fluorescence, when dyes are in the hot-spot but not directly adsorbed on the metal surface. Despite the much shorter distance of the fluorophore to the metal surface than typically used (5−20 nm[5−7]), large SEF enhancements are nevertheless predicted and observed[28,29] in such gap-containing systems. While our previous study put the emphasis on the theory behind the phenomenon, and the effect of the original quantum yield on the observed enhancement, it was limited to a single excitation wavelength (532 nm) which is close to the plasmon peak position very early in the aggregation process. This allowed us to achieve a moderately high fluorescence enhancement only for a short period of time and prevented us from getting reliable corroborative data such as fluorescence lifetime measurements to make an estimate of the field enhancement involved in the process. Here we discuss the time-dependent evolution of the average plasmon-interaction peak during aggregation and its effect on the average enhancement of fluorescence. The average plasmon peak reaches an almost constant value after a few minutes, which enabled us to demonstrate large and stable enhancement of the average fluorescence of more than 150 times. As far as we know, this is the highest published *average* fluorescence enhancement to date and is comparable with the best-reported values for single-molecule SEF (when correcting for the effect of the fluorescence quantum yield QY, see below). Moreover, we show that such large enhancements are concomitant with extreme reduction (>300×) of the observed fluorescence lifetime.

■ MATERIALS AND METHODS

Reagents. Atto 655 (A655) dye-labeled DNA and non-labeled control had the following sequence: 5′-dye-TGGAAGTTAGATTGGGATCATAGCGTCAT-3′. These oligonucleotides were custom synthesized by IBA GmbH (Göttingen, Germany). All other chemicals were purchased from Sigma-Aldrich.

Nanoparticle Synthesis. EDTA-coated Ag nanoparticles were synthesized according to a modified literature procedure:[30] In brief, 500 mL of a 0.16 mM EDTA solution containing 4 mM NaOH was heated to boiling under stirring. 5 mL of 26 mM AgNO$_3$ solution was added in four aliquots of 1.25 mL, and the solution was held at boiling for 20 min with continuous stirring.

Time-Dependent Absorption Measurements. Fast absorbance spectral measurement was done by a CCD-based spectrometer. Light from an AvaLight-Hal light source (Avantes, The Netherlands) is coupled into a 50 μm multimode fiber (Thorlabs M14L01) and is coupled in a fiber-based cuvette holder (Thorlabs CVH100) with mounted optical filters (BG 40-IR and Roscolux #71). Transmitted light from the cuvette is coupled to a photospectrometer (Ocean Optics QE65000) by use of second fiber. Custom LabView

software for the spectrometer allows for single or repetitive measurements with a fixed time interval. The dynamic range is limited by the 16 bit depth of the spectrometer. Intensity compensation is necessary to maintain a good dynamic range over the full wavelength range. Compensation of the light source was achieved using a BG 40-IR filter, while compensation for the spectrometer efficiency was achieved using a Roscolux #71 Sea Blue filter. All measurements were done with 0.5 s integration time. Spectra were corrected for dark noise and absorption was measured relative to a blank (cuvette with buffer only). The peak wavelength was extracted from the data by fitting a sixth-order polynomial to the area around the peak and using the peak position from the fitted curve.

Measurement of Fluorescence. Fluorescence was measured using a Tecan Safire II fluorescence plate reader equipped with a Quad4 monochromator.

SEF Measurements. For SEF measurements, as-synthesized Ag-nanoparticles were diluted in 6 mM phosphate buffer, pH = 7.1, to a concentration equivalent to 1.6 OD (as measured in a 10 mm path length cuvette). 40 μL of 2.5 nM dye-DNA diluted in water was mixed with 40 μL of 100 μM spermine in 10 mM Tris buffer (pH = 7.4), and then 120 μL of the diluted Ag nanoparticles was added. The final concentration of dye-labeled DNA was 500 pM.

Calculation of the Quantum Yields of Dyes. The calculation of quantum yield for A655 attached to DNA and for free A655 was done in a similar fashion to that previously reported by us.[28] We used sulforhodamine 101 dye in ethanol as the reference dye (assuming QY of 0.95[31]). All fluorescent emission measurements for QY calculation were carried out on a Cary Eclipse fluorescence spectrometer (Varian).

Time-Resolved Fluorescence. Time-resolved fluorescence spectra were recorded with a subpicosecond streak-camera system combined with a grating (50 grooves/mm, blaze wavelength 600 nm) with the central wavelength set at 700 nm, having a spectral width of 260 nm (for details see refs 32 and 33). Vertically polarized excitation pulses of ∼100 fs and 615 nm were used to excite the sample; the spot size diameter was typically ∼100 μm, and the laser repetition rate was 250 kHz. The detector polarizer was set at the magic angle orientation, and a time range of 800 ps was used. To minimize the scattering from the sample, two long pass filters with cut-on wavelength of 630 and 645 nm were added between the sample and detector. For scattering signal only, the second filter was removed. Streak images were obtained and corrected for background and photocathode shading and then sliced up into traces of 4 nm width.

Data Analysis of Time-Resolved Measurements. Data obtained with the streak-camera setup were analyzed in two different ways: (i) global analysis with the R package TIMP with the IRF being determined by the software (for details see refs 34 and 35) and (ii) analysis of averaged decay curves which cover the wavelength range of 680 ± 10 nm. Here, we used the scattering beam as our instrument response function (IRF), and custom-written software was used to do the deconvolution.[36] Analysis i provides us the decay associated spectra (DAS), while analysis ii was used to determine lifetimes.

■ RESULTS AND DISCUSSION

Figure 1 shows a schematic representation of the experiment. Silver nanoparticles (34 nm average size) and a dye-labeled DNA are coaggregated by the introduction of spermine, a
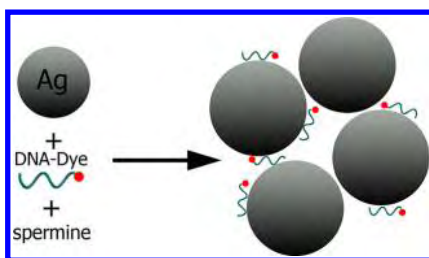
Figure 1. Spermine-induced coaggregation of dye-labeled DNA and Ag nanoparticles.

polycationic small molecule. Note that the results presented here are not specific to the particular DNA sequence or fluorophore chosen, although minor changes are expected for other choices.[28] The aggregation of negatively charged metallic nanoparticles by positively charged small molecules is a dynamic process, which leads to an increase in cluster size with time. However, the plasmonic properties of the aggregate evolve much more slowly, as the effect of an incremental increase in the size of the aggregate causes a diminishing red-shift in the observable plasmon resonance. Figure 2a shows the time-dependent absorption spectra of Ag nanoparticles after their addition to a solution containing the aggregating agent spermine. The single particle plasmon peak at 410 nm stays at a constant wavelength and its amplitude decreases with time, while the second, red-shifted peak, arising from particle–particle plasmon interactions, continues to red-shift as the aggregation progresses. This red-shift of the interaction peak is rather large in the first minute of aggregation, but it asymptotically approaches a constant level after a few minutes. This can be seen more clearly in Figure 3a showing the position of the average interaction plasmon peak vs time. A detailed explanation for a very similar process in gold nanoparticle aggregation was recently given by Taylor et al.[37] We expect our silver nanoparticle aggregation to follow a similar diffusion-limited dynamics, as our aggregating agent (spermine) is present in high excess compared to the nanoparticles (10^6:1). This excess gives a very fast initial aggregation, followed by a very slow second phase of the red-shifting of the plasmon interaction peak. The effect is also captured, at least qualitatively, in theoretical predictions of the plasmon

resonance of a linear chain of closely spaced metallic spheres as a function of chain length, as shown in Figure 2b. Our experimental results are consistent with these predictions, although the actual resonances are at a slightly longer wavelength due to the 3D nature of the aggregates (as opposed to the 1D chains considered in the simulation).

As the extinction peak of the interaction plasmon shifts rapidly and then becomes stable, one would also expect to see such stabilization in the fluorescence enhancement. For SEF experiments, we chose a fluorophore—Atto-655 (A655)—with excitation and emission peaks very close to the wavelength where the interaction plasmon stabilizes (670 nm) to achieve high fluorescence enhancement (see Figure S3 in Supporting Information). The average SEF enhancement factor was measured as the ratio of the fluorescence intensity from a solution including dye-labeled DNA, silver nanoparticles, and aggregating agent to that of a similar solution but without the aggregating agent, as explained previously.[28] The change in fluorescence enhancement with time can be seen in Figure 3b. In the first few minutes, as the interaction plasmon shifts to the red and comes closer to the excitation and emission wavelength we have used, one can see that the fluorescence enhancement increases. In parallel to the stabilization of the plasmon peak, we see a similar stabilization in the enhancement factor. The slight decrease in the fluorescence enhancement after 100 s, which was experimentally verified not to be caused by photobleaching, is attributed to the decrease in the extinction at the excitation wavelength, as explained below.

These observations can be further analyzed within the framework of the electromagnetic theory of SEF, from which we here only use a simplified version and highlight below the most relevant features (see Supporting Information and refs 21, 29, and 39−41 for further details). The fluorescence intensity is affected by the metal nanoparticles in two ways. First, the excitation process is enhanced by the local field intensity enhancement factor at the excitation wavelength λ_L, which we denote $M_{Loc}(\lambda_L)$. In addition, the quantum yield for emission is also modified (compared to the native quantum yield Q_0) and can be approximated as[29,41] $Q = M_{Rad}(\lambda_R)/M_{Tot}$, where M_{Tot} is the total decay rate enhancement factor (with respect to the native radiative rate) and $M_{Rad}(\lambda_R)$ is the radiative enhancement factor (at the emission wavelength λ_R). Moreover, due to
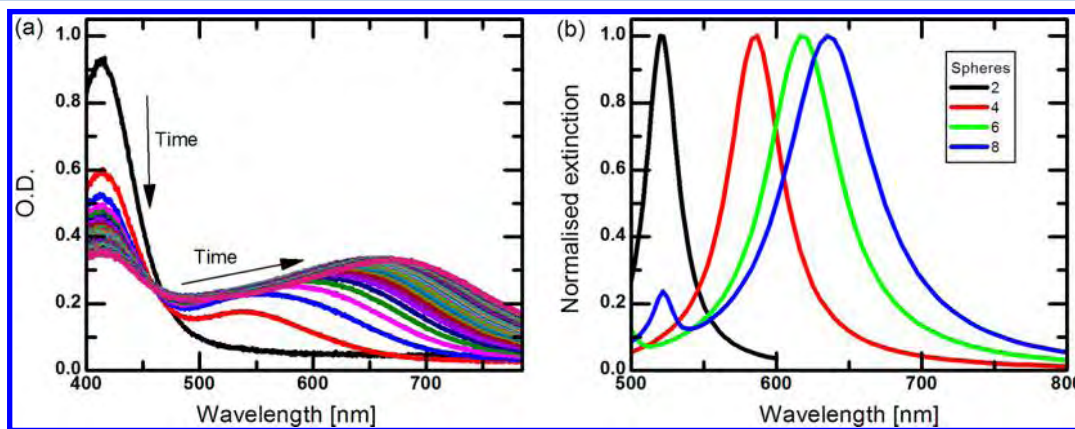

Figure 2. (a) UV−vis spectra of the nanoparticle aggregation with time. Spectra measured every 5 s for the first 5 min of aggregation. The experiment was performed using 100 pM Ag nanoparticles, 500 pM DNA, and 100 μM spermine, except for the top (black) spectrum obtained without aggregating agent. (b) Predicted normalized extinction (absorption + scattering) spectra of silver nanoparticle chains with 34 nm particle diameter and 1.5 nm particle spacing for different number of spherical nanoparticles in the chain. These results were obtained from full electrodynamics calculations carried out using finite element modeling[38] (see Supporting Information for details).
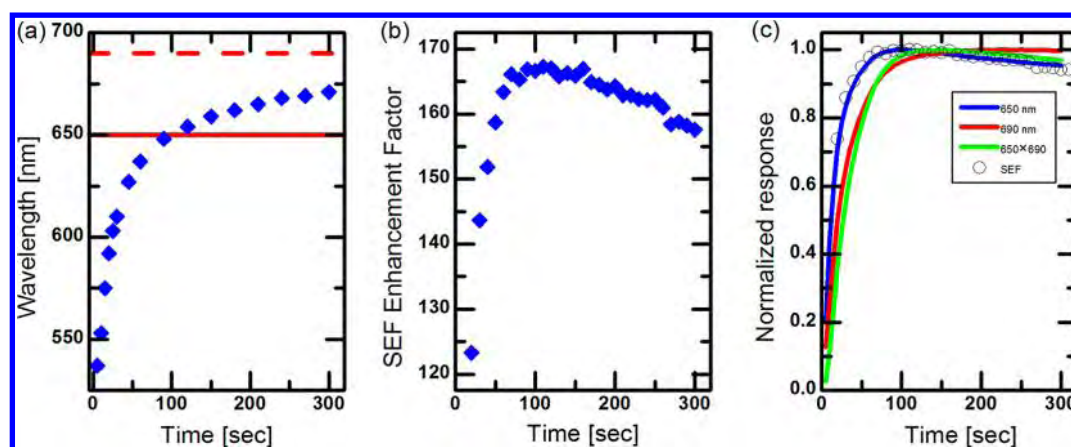
Figure 3. (a) Peak wavelength of aggregate plasmon resonance as a function of aggregation time. The red solid line represents the excitation wavelength used for the measurement (650 nm with 9 nm bandwidth), and the red broken line represents the emission wavelength used (690 nm with 20 nm bandwidth). (b) Average fluorescence enhancement factor (the ratio of fluorescence in the presence of silver nanoparticles and aggregation agent vs the fluorescence in the absence of silver nanoparticles) vs aggregation time. (c) Normalized value for the SEF intensity (circles), extinction averaged over 650 ± 4.5 nm (blue line), extinction averaged over 690 ± 10 nm (red line), and product of the two normalized extinction values (green line). All experiments were conducted in a solution containing 500 pM of A655-labeled DNA, 20 mM spermine, and 4 mM phosphate buffer pH = 7.1. The NPs concentration was 100 pM. Error bars were omitted due to clarity but were all smaller than or equal to the marker size (see Supporting Information for further details on the reproducibility of the measurements).

optical reciprocity,[42] we can also approximate $M_{Rad}(\lambda_R)$ by $M_{Loc}(\lambda_R)$, which is expected to follow the extinction at $\lambda_R = 690$ nm. We therefore obtain for the fluorescence enhancement factor the simplified expression

$$M_{SEF} = [M_{Loc}(\lambda_L)M_{Loc}(\lambda_R)]/(Q_0 M_{Tot}) \qquad (1)$$

This expression justifies the use of the product $Q_0 \times M_{SEF}$ as a fluorophore-independent figure of merit for the SEF enhancement and not just M_{SEF} because in that case experiments with poor fluorophores (i.e., with small Q_0) would result in artificially inflated fluorescence enhancement. In our aggregation experiments, the local field intensity factor, $M_{Loc}(\lambda)$, should change with time as the plasmon peak red-shifts, and this variation is approximately proportional to the measured extinction at the corresponding wavelength λ[43,44] (see also Supporting Information for further justification). Moreover, the factor M_{Tot} can be decomposed into its radiative contribution (essentially M_{Rad}), which follows the spectral profile of the plasmon resonance, and its nonradiative contribution M_{NR}, which is not strongly geometry- and wavelength-dependent. When the latter dominates (in particular, for molecules directly adsorbed on the metal), the fluorescence enhancement factor should be qualitatively proportional to the product of the extinction at $\lambda_L = 650$ nm and $\lambda_R = 690$ nm. However, if the radiative contribution dominates (i.e., $M_{NR} \ll M_{Rad}(\lambda_R)$), then the fluorescence enhancement reduces to $M_{SEF} \approx \eta M_{Loc}(\lambda_L)/Q_0$, where the modified quantum yield $\eta = M_{Rad}/M_{Tot}$ does not depend strongly on λ_R (and $\eta \approx 0.4$; see Supporting Information). M_{SEF} should then follow the variation of the extinction at $\lambda_L = 650$ nm only. (See Supporting Information for the comparison of M_{Rad} and η spectral characteristics for the model case of a nanoparticle dimer.) In Figure 3c, we observe a very good agreement between the time dependence of the SEF signal and that of the extinction at 650 nm (but not with that of the product of extinctions). We therefore conclude that the radiative contribution dominates the total decay rate enhancement factor. This arises in our system from a combination of two effects. First, the DNA-labeled fluorophores are not directly adsorbed on the surface and are therefore slightly further away

from the NP surface, which reduces to some extent the magnitude of the nonradiative enhancement factor M_{NR}. We estimate the distance to the surface to be of the order of $d = 1.5-2$ nm (as inferred from TEM images[28]), which corresponds to M_{NR} of the order of 130–650 (eq S4 in the Supporting Information). Second, the local field enhancement and radiation enhancement can be very large in our system, in particular for molecules close to the gaps between particles (so-called hot-spots). For these, M_{Rad} as large as 10^4 is predicted from EM calculations at the plasmon resonance. It is likely that due to steric hindrance, DNA-labeled fluorophores do not actually reach the gap in between two NPs but only approach it. Even then, relatively large enhancement factors, $M_{Rad} \approx 3000$, are predicted in the vicinity of the hot-spot (for example, 20° off-axis; see Supporting Information). Since those molecules at (or close to) hot-spots dominate the SEF signal, one can reasonably expect that the radiative contribution dominates M_{Tot}, as indeed measured. This is in sharp contrast with experiments where the SEF spectral dependence followed the product of extinction at excitation and detection wavelengths.[39] In this latter case, the molecules were directly adsorbed on the metal and nonradiative decay dominated the factor M_{Tot}. In fact, M_{Tot} as large as 4×10^5 has been measured in this context.[41]

In order to further confirm these interpretations, we carried out fluorescence lifetime measurements in our system to determine the order of M_{Tot}. Although very strong reduction of the observed lifetime is predicted to coexist with high fluorescence intensity enhancement,[45] the actual measurement of lifetime in parallel to the intensity enhancement in SEF is rare, and in most cases the changes in lifetime measured were less than 1 order of magnitude.[10,17,46] Only a few examples exist for higher lifetime reduction near metallic structures (while still having enhancement of the fluorescence intensity), but they too were no higher than ∼30×.[7,47,48]

Using a time-correlated single photon counting (TCSPC)-based lifetime system, the average lifetime of the A655-labeled DNA in solution was measured to be 1.8 ± 0.1 ns (see Figure 4a). When the same A655-labeled DNA was mixed with the
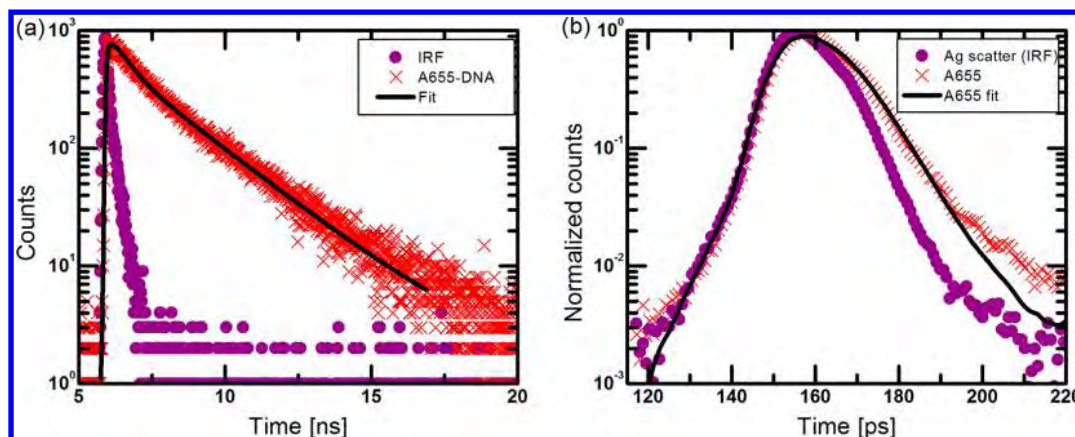
Figure 4. (a) Fluorescence lifetime measurement for A655 dye in the absence of silver nanoparticles (red ×) and fit (black curve). These data were measured on a TCSPC-based system. (b) Fluorescence lifetime measurement of A655 dye in the presence of silver nanoparticles and aggregating agent (red ×) and fitted (black) curve. This graph was measured on a streak camera based system.[32]

silver nanoparticles and aggregating agent, we could not quantify the lifetime of the enhanced fluorescence, as the observed signal was indistinguishable from our instrument response function (IRF). However, unlike many previous systems where only a single fluorophore is enhanced, we are enhancing many fluorophores in the solution. We were therefore able to use a streak camera to measure both spectrum and lifetime with very high temporal resolution (see Supporting Information for more details).

The fit of the lifetime measurement using the streak camera gives 6.0 ± 0.8 ps, which corresponds to a lifetime reduction of 300× (Figure 4b), *an order of magnitude larger than any previously reported value for a system that shows enhanced fluorescence.* We can moreover estimate the native radiative lifetime for this dye from the measured photophysical data of the dye in water to be about 6 ns (30% QY and 1.8 ns lifetime). This would indicate that the brightest dyes experience a total decay rate enhancement factor of $M_{Tot} \sim 1000$, in agreement with the theoretical estimates assuming that the fluorophores are 1.5–2 nm away from the surface and cannot fully reach the gap between particles.

A semiquantitative analysis of the various EFs in our system can also be carried out as follows. Taking into account the earlier observation that M_{Tot} is dominated by its radiative component, we also deduce that the local field intensity enhancement M_{Loc} for the brightest dyes (closest to the hot-spot) is of the order of $M_{Loc} \approx \eta M_{Tot} \sim 400$. Using the unrealistic assumption that all dyes are contributing equally to the enhancement (i.e., they are all as close as possible to the hot-spots), this would imply that the average fluorescence EF is of the order of $M_{SEF} \approx \eta M_{Loc}/(Q_0) \sim 1250$, which therefore represents the upper limit for this system. The lower observed average fluorescence enhancement of around 150 can therefore be explained by assuming that only ~12% (150/1250) of the fluorophores in the aggregates contribute dominantly to the SEF signal. This conclusion is similar to that obtained from SERS experiments in aggregated colloidal systems[19,26,27] and originates from the distribution of enhancement factor, which varies dramatically on the surface as one moves away from the hot-spot, resulting in a small fraction of the molecules (those closest to the hot-spot, probably of the order of 10% in our case) contributing to the majority of the SEF signal.

In order to compare our results to those we have achieved previously and to the available literature, it should be noted that following eq 1 the fluorescence enhancement factor (EF) is inversely dependent on the original quantum yield of the fluorophore (Q_0), and therefore it cannot serve as a good figure of merit for comparison between experiments done using different dyes. However, a more general figure of merit for SEF experiments would be the product of the fluorescence enhancement factor with the quantum yield of the fluorophore (under nonenhanced condition), i.e., the quantity FoM = $M_{SEF}Q_0$. Indeed, the electromagnetic model for SEF predicts[29,40] that this FoM is approximately independent of the fluorophore under study and is therefore an intrinsic property quantifying the SEF performance of a given substrate. Our previous results[28] provide a good illustration of this: different dyes with different Q_0, and different charges gave fluorescence EFs over a wide range (9–740×) despite being measured in the same plasmonic system. However, when considering our suggested FoM, all results fall in the range of 1–3, which is much narrower, with the spread probably coming out of small differences in orientations and distances from the surface that depend on the exact chemical nature of the dyes used. For the measurements described in this article, the corresponding FoM is 22 ± 3, which is to the best of our knowledge the highest FoM for average fluorescence enhancement reported to date. In fact, it is even comparable to the highest reported single-molecule fluorescence enhancement FoM of 33 obtained by the Moerner group[47] using bow-tie gap antennas. These figures demonstrate the remarkable potential of aggregated silver colloidal systems as highly efficient surface-enhanced fluorescence substrates.

■ CONCLUSION

In conclusion, we show that coaggregation of silver nanoparticles with dye-labeled DNA creates nanoparticle aggregates with entrapped dye molecules, which effectively behave as self-assembled nanoantennas. For A655-DNA, with a QY of 13 ± 2%, an average enhancement of the fluorescence intensity of 170× (corresponding to a figure of merit of 22 ± 3 for the average SEF) was observed together with a lifetime reduction of 300×. These two observations are consistent with the electromagnetic model of fluorescence, assuming that the molecules are at a distance of approximately 1.5–2 nm from the surface, and the fact that a small fraction (~10%) of the molecules, those closest to hot-spots, contribute to the majority of the SEF signal. If schemes for site-selective adsorption of

16691

dx.doi.org/10.1021/jp305720q | J. Phys. Chem. C 2012, 116, 16687–16693

fluorophores at or in the vicinity of the hot-spots were implemented in this system (as was recently reported for SERS[49]), then even larger average fluorescence enhancements are potentially achievable. Thus, this self-assembly-based nanoantenna generation can open new avenues in plasmonic enhancement applications in analytical sciences, where a large enhancement of the average fluorescence can lead to more sensitive detection of fluorescent molecules.

■ ASSOCIATED CONTENT

Ⓢ Supporting Information

An explanation regarding the reproducibility of measurements, detailed results of streak camera measurements and controls, position of excitation and emission wavelengths in comparison to the excitation and emission spectra of A655-DNA, SEF control experiments, finite-element modeling, and electromagnetic calculations based on the dimer model. This material is available free of charge via the Internet at http://pubs.acs.org.

■ AUTHOR INFORMATION

Corresponding Author

*E-mail r.gill@utwente.nl; Fax +31-53-4891105; Ph +31-53-4893067.

Notes

The authors declare no competing financial interest.

■ ACKNOWLEDGMENTS

■ REFERENCES

(1) Crozier, K. B.; Sundaramurthy, A.; Kino, G. S.; Quate, C. F. *J. Appl. Phys.* **2003**, *94*, 4632–4642.
(2) Novotny, L.; van Hulst, N. *Nat. Photonics* **2011**, *5*, 83–90.
(3) Seok, T. J.; Jamshidi, A.; Kim, M.; Dhuey, S.; Lakhani, A.; Choo, H.; Schuck, P. J.; Cabrini, S.; Schwartzberg, A. M.; Bokor, J.; Yablonovitch, E.; Wu, M. C. *Nano Lett.* **2011**, *11*, 2606–2610.
(4) Ahmed, A.; Gordon, R. *Nano Lett.* **2011**, *11*, 1800–1803.
(5) Fort, E.; Grésillon, S. *J. Phys. D: Appl. Phys.* **2008**, *41*, 013001.
(6) Anger, P.; Bharadwaj, P.; Novotny, L. *Phys. Rev. Lett.* **2006**, *96*, 113002.
(7) Kühn, S.; Håkanson, U.; Rogobete, L.; Sandoghdar, V. *Phys. Rev. Lett.* **2006**, *97*, 017402.
(8) Tam, F.; Goodrich, G. P.; Johnson, B. R.; Halas, N. J. *Nano Lett.* **2007**, *7*, 496–501.
(9) Bardhan, R.; Grady, N. K.; Halas, N. J. *Small* **2008**, *4*, 1716–1722.
(10) Bardhan, R.; Grady, N. K.; Cole, J. R.; Joshi, A.; Halas, N. J. *ACS Nano* **2009**, *3*, 744–752.
(11) Ming, T.; Zhao, L.; Yang, Z.; Chen, H.; Sun, L.; Wang, J.; Yan, C. *Nano Lett.* **2009**, *9*, 3896–3903.
(12) Bharadwaj, P.; Anger, P.; Novotny, L. *Nanotechnology* **2007**, *18*, 044017.
(13) Zhang, J.; Malicka, J.; Gryczynski, I.; Lakowicz, J. R. *J. Phys. Chem. B* **2005**, *109*, 7643–7648.
(14) Ringler, M.; Schwemer, A.; Wunderlich, M.; Nichtl, A.; Kurzinger, K.; Klar, T. A.; Feldmann, J. *Phys. Rev. Lett.* **2008**, *100*, 203002.
(15) Jain, P. K.; Huang, W.; El-Sayed, M. A. *Nano Lett.* **2007**, *7*, 2080–2088.
(16) Xu, H. X.; Wang, X. H.; Persson, M. P.; Xu, H. Q.; Käll, M.; Johansson, P. *Phys. Rev. Lett.* **2004**, *93*, 243002.
(17) Bakker, R. M.; Drachev, V. P.; Liu, Z.; Yuan, H.-K.; Pedersen, R. H.; Boltasseva, A.; Chen, J.; Irudayaraj, J.; Kildishev, A. V.; Shalaev, V. M. *New J. Phys.* **2008**, *10*, 125022.
(18) Johansson, P.; Xu, H. X.; Käll, M. *Phys. Rev. B* **2005**, *72*, 035427.
(19) Le Ru, E. C.; Etchegoin, P. G.; Meyer, M. *J. Chem. Phys.* **2006**, *125*, 204701.
(20) Stranahan, S. M.; Willets, K. A. *Nano Lett.* **2010**, *10*, 3777–3784.
(21) Creighton, J. A.; Blatchford, C. G.; Albrecht, M. G. *J. Chem. Soc., Faraday Trans. 2* **1979**, *75*, 790–798.
(22) Larmour, I. A.; Faulds, K.; Graham, D. *J. Raman Spectrosc.* **2012**, *43*, 202–206.
(23) Kneipp, K.; Wang, Y.; Kneipp, H.; Perelman, L. T.; Itzkan, I.; Dasari, R. R.; Feld, M. S. *Phys. Rev. Lett.* **1997**, *78*, 1667–1670.
(24) Nie, S.; Emory, S. R. *Science* **1997**, *275*, 1102–1106.
(25) Xu, H. X.; Bjerneld, E. J.; Käll, M.; Börjesson, L. *Phys. Rev. Lett.* **1999**, *83*, 4357–4360.
(26) Le Ru, E. C.; Meyer, M.; Etchegoin, P. G. *J. Phys. Chem. B* **2006**, *110*, 1944–1948.
(27) Le Ru, E. C.; Etchegoin, P. G. *Annu. Rev. Phys. Chem.* **2012**, *63*, 65–87.
(28) Gill, R.; Le Ru, E. C. *Phys. Chem. Chem. Phys.* **2011**, *13*, 16366–16372.
(29) Le Ru, E. C.; Etchegoin, P. G. *Principles of Surface Enhanced Raman Spectroscopy and Related Plasmonic Effects*; Elsevier: Amsterdam, 2009.
(30) Heard, S. M.; Grieser, F.; Barraclough, C. G.; Sanders, J. V. *J. Colloid Interface Sci.* **1983**, *93*, 545–555.
(31) Velapoldi, R.; Tønnesen, H. *J. Fluoresc.* **2004**, *14*, 465–472.
(32) Tian, L.; van Stokkum, I. H. M.; Koehorst, R. B. M.; Jongerius, A.; Kirilovsky, D.; van Amerongen, H. *J. Am. Chem. Soc.* **2011**, *133*, 18304–18311.
(33) Stokkum, I. H. M.; Oort, B.; Mourik, F.; Gobets, B.; Amerongen, H. In *Biophysical Techniques in Photosynthesis*; Aartsma, T. J., Matysik, J., Eds.; Springer: Dordrecht, The Netherlands, 2008; Vol. *26*, pp 223–240.
(34) Laptenok, S. P.; Borst, J. W.; Mullen, K. M.; van Stokkum, I. H. M.; Visser, A. J. W. G.; van Amerongen, H. *Phys. Chem. Chem. Phys.* **2010**, *12*, 7593–7602.
(35) Mullen, K. M.; van Stokkum, I. H. M. *J. Stat. Softw.* **2007**, *18*, 1–46.
(36) van Oort, B.; Alberts, M.; de Bianchi, S.; Dall'Osto, L.; Bassi, R.; Trinkunas, G.; Croce, R.; van Amerongen, H. *Biophys. J.* **2010**, *98*, 922–931.
(37) Taylor, R. W.; Lee, T.-C.; Scherman, O. A.; Esteban, R.; Aizpurua, J.; Huang, F. M.; Baumberg, J. J.; Mahajan, S. *ACS Nano* **2011**, *5*, 3878–3887.
(38) Khoury, C. G.; Norton, S. J.; Vo-Dinh, T. *ACS Nano* **2009**, *3*, 2776–2788.
(39) Le Ru, E. C.; Etchegoin, P. G.; Grand, J.; Félidj, N.; Aubard, J.; Lévi, G. *J. Phys. Chem. C* **2007**, *111*, 16076–16079.
(40) Weitz, D. A.; Garoff, S.; Gersten, J. I.; Nitzan, A. *J. Chem. Phys.* **1983**, *78*, 5324–5338.
(41) Galloway, C. M.; Etchegoin, P. G.; Le Ru, E. C. *Phys. Rev. Lett.* **2009**, *103*, 063003.
(42) Le Ru, E. C.; Etchegoin, P. G. *Chem. Phys. Lett.* **2006**, *423*, 63–66.
(43) Le Ru, E. C.; Grand, J.; Félidj, N.; Aubard, J.; Lévi, G.; Hohenau, A.; Krenn, J. R.; Blackie, E.; Etchegoin, P. G. *J. Phys. Chem. C* **2008**, *112*, 8117–8121.
(44) Messinger, B. J.; von Raben, K. U.; Chang, R. K.; Barber, P. W. *Phys. Rev. B* **1981**, *24*, 649–657.
(45) Mohammadi, A.; Kaminski, F.; Sandoghdar, V.; Agio, M. *J. Phys. Chem. C* **2010**, *114*, 7372–7377.

(46) Muskens, O. L.; Giannini, V.; Sánchez-Gil, J. A.; Gómez Rivas, J. *Nano Lett.* **2007**, *7*, 2871−2875.

(47) Kinkhabwala, A.; Yu, Z. F.; Fan, S. H.; Avlasevich, Y.; Müllen, K.; Moerner, W. E. *Nat. Photonics* **2009**, *3*, 654−657.

(48) Li, J.; Wang, Z.; Gryczynski, I.; Mandecki, W. *Anal. Bioanal. Chem.* **2010**, *398*, 1993−2001.

(49) Le Ru, E. C.; Grand, J.; Sow, I.; Somerville, W. R. C.; Etchegoin, P. G.; Treguer-Delapierre, M.; Charron, G.; Félidj, N.; Lévi, G.; Aubard, J. *Nano Lett.* **2011**, *11*, 5013−5019.

Supporting Information for "Silver nanoparticle aggregates as highly efficient plasmonic antennas for fluorescence enhancement"

Ron Gill[a], Lijin Tian[b] , Walter R. C. Somerville[c], Eric C. Le Ru[c], Herbert van Amerongen[b,d],*
Vinod Subramaniam[a]

[a] Nanobiophysics Group, MIRA Institute for Biomedical Technology and Technical Medicine, University of Twente, PO Box 217, 7500 AE Enschede, The Netherlands

[b] Laboratory of Biophysics, Wageningen University, P.O. Box 8128, 6700 ET, Wageningen, The Netherlands

[c] The MacDiarmid Institute for Advanced Materials and Nanotechnology, School of Chemical and Physical Sciences, Victoria University of Wellington, P.O. Box 600, Wellington 6140, New Zealand

[d] MicroSpectroscopy Centre, Wageningen University, P.O. Box 8128, 6700 ET, Wageningen, The Netherlands

I. EXPERIMENTAL DETAILS

Reproducibility of measurements:

Unlike single molecules experiment on SEF, were shot noise and other noise source are significant compared to the signal level, in this system all our signals are rather high. This provides a very low intrinsic noise level to our measurements, and as we have shown previously[1] we can get less than 1% coefficient of variation (CV) on repeat experiments. From a practical point of view, because of the limited dynamic range of photodetectors, when the enhanced fluorescence is below the saturation level of the detector, the fluorescence measurement of the water sample and the dye only sample are low and suffer from noise. However these two samples are not changing with time, so we average the different time measurements on these samples to get high accuracy. One factor that is important in the measurement is the temperature. The dependence of aggregation on temperature is known from literature, [2] and therefore we conduct all our experiments at room temperature, which is kept constant at the lab at 22°C. It is important to note that it is not the optimal temperature, since in several experiments where the stock solutions were used when they are still cold from the fridge, the intensity enhancement factor was measured to be 10-15% higher that the result reported in this paper. However, in such experiments, the correlation to the aggregation kinetics that was measured independently (and at probably a slightly different temperature of the reactants) was not as good as when all were measured at the same (room) temperature.

Time resolved fluorescence measurements on Silver nanoparticle-dye complexes

In order to confirm that we can use the scattering beam as our instrument response function (IRF), we compared the decay curve of A655-DNA in the presence of silver nanoparticles and aggregating agent to the time response of pinacyanol in methanol (measured under the same conditions) which was previously determined to have a 6 ps lifetime[3]. As can be seen in Figure S1, the decay of A655-DNA, which gives a lifetime of 6 ps when the scattering curve is used as the IRF, overlaps with the decay curve of pinacyanol.
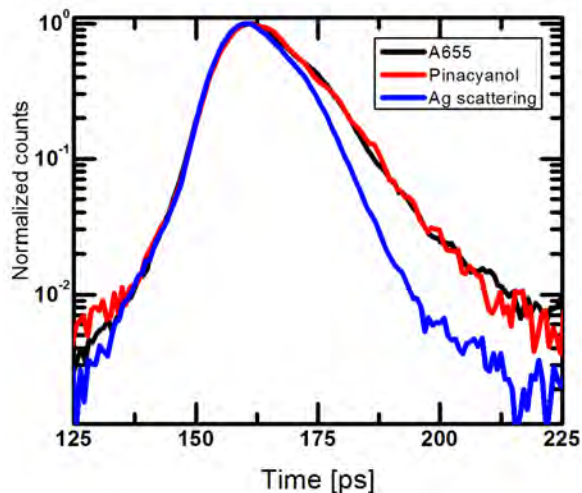
Figure S1: Decay curves of 680 nm±10 nm. A655 with Ag-NPs and spermine (black), pinacyanol (red), and Ag scattering (blue). For comparison, all traces are normalized to their maxima and horizontally shifted from the original data to the same starting point.

Figure S2 shows the emission spectra of A655-DNA co-aggregated with Ag-NPs as measured in the fluorescence spectrometer, in comparison to that measured by the streak camera. A good agreement is found between the two. In the streak camera system, when the second 645 nm long pass filter is removed, a very strong scattering peak (~100× stronger than the fluorescence peak at 680 nm) with a spectral dependence that corresponds to the laser, rather than the fluorescence emission is detected (Figure S2, black line). The time decay of this data around 615 nm was used as the IRF of the instrument.
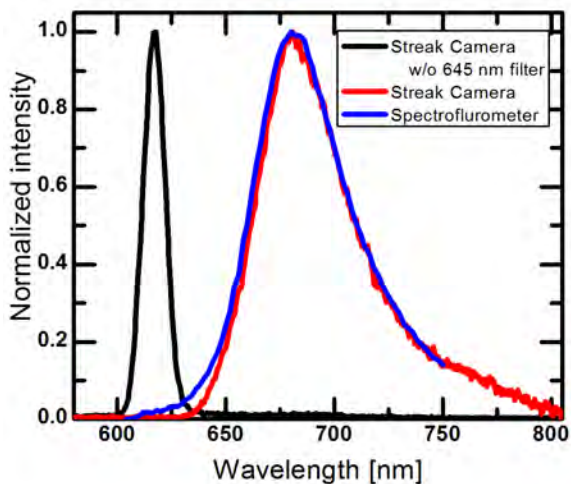

Figure S2: Spectrum of A655-DNA with Ag-NPs and spermine: as measured on the Tecan Safire II spectrometer (blue), as measured by the streak camera using both a 630nm and a 645nm long pass filter (red) and as measured by the streak camera with only the 630nm long pass filter (black).

Excitation and emission wavelength position when measuring SEF compared to the absorption and emission spectra of A655-DNA
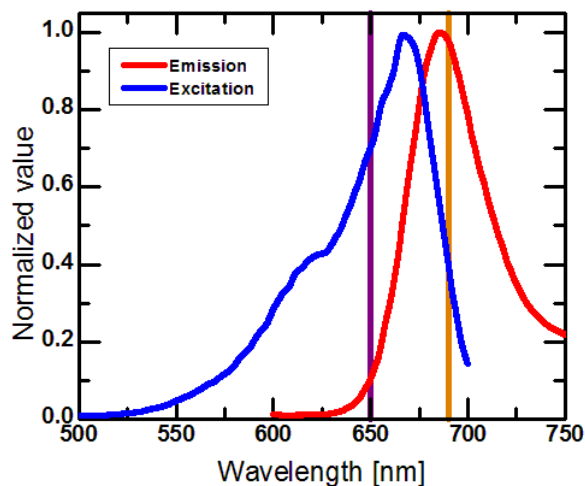

Figure S3: Excitation and emission spectra of the A665-DNA. The purple line marks the center position of the excitation monochromator used in the SEF experiments (650nm) and the orange line marks the center position of the emission monochromator used in the SEF experiments (690nm).
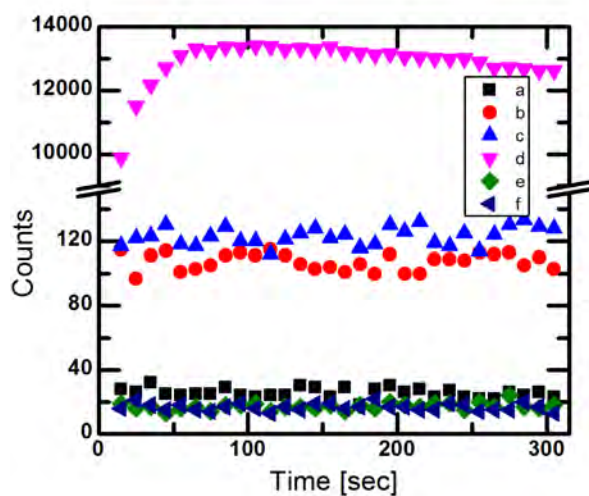
Control experiments

Figure S4: Time dependence of fluorescence readout for a) pure water; b) no aggregating agent and no silver control (only dye); c)no silver control (dye and aggregating agent); d) full experiment containing dye-labeled

DNA, aggregating agent and silver nanoparticles; e) no-DNA control (only spermine and Ag nanoparticles); f) no dye control (unlabelled DNA, spermine and Ag nanoparticles). In all experiments final dye concentration is 0.5 nM, final spermine concentration is 100 μM and final silver concentration is 100 pM.

II. THEORETICAL CONSIDERATIONS

Finite Element Modeling electromagnetic calculations

In order to understand the effect of increasing aggregation of nanoparticles, simulations were carried out using the commercial software COMSOL[http://www.comsol.com/, version 4.2]. This software uses Finite Element Modeling to calculate electromagnetic properties. The simulations were carried out in 3D, using the frequency domain study of the Electromagnetic Waves physics interface, which is implemented in the RF module. The spheres in the simulation were of radius r=17 nm, with gaps of g=1.5 nm. The simulations used the dielectric function of silver from Ref. [4] and NPs were embedded in water with n=1.33. The spheres are arranged in a linear chain for simplicity, and the incident field is polarized along the chain axis and is propagating perpendicular to it. The chain was enclosed in a spherical bounding box of radius 680 nm, which was surrounded by a spherical perfectly matched layer (PML) with 6 layers and total thickness of 520 nm. The purpose of the PML is to eliminate reflections from the boundary of the simulation volume. Convergence of the results was tested by comparing the results from the dimer to exact results obtained from generalized Mie theory[5-7].

Electromagnetic calculations based on the dimer model

In order to understand, at least semi-quantitatively, the main features of the electromagnetic model for SEF in our system, we have used the model system of a dimer of two closely-spaced silver nanoparticles. This provides a simplified model of our aggregates, which nevertheless captures the most important physical phenomena associated with gap-containing nanostructures. For this model, all the necessary electromagnetic properties can be calculated efficiently and accurately within the framework of generalized Mie theory (see [5-7] for details). In aggregates bigger than a dimer, plasmon resonances are typically redshifted (as in the example of a chain also studied in this work) and damped. As a result, this simplified model cannot predict the position of the plasmon resonance and is also likely to overestimate local field enhancements. With these provisos in mind, it does however allow us to clarify and illustrate on simple examples the concepts that are discussed in the main paper. It is with this

goal in mind that we provide the following figures and discussion (see also the supplementary information of [8] for further details).

The parameters used for the calculations have been chosen to match those estimated in our real system. We therefore consider silver spheres (with the dielectric function of[4]) of radius a=17 nm (34 nm diameter), separated by a gap of g=1.5 nm and embedded in water (n=1.33). The incident wavelength, λ_L, is the main parameter. We here only consider excitation polarized along the dimer axis (and propagating perpendicular to it). This is the situation where a maximum coupling to the main (most redshifted) plasmon resonance of the dimer occurs. In reality, orientation averaging should be carried out, which would typically result in lower average enhancements[9,10].

We first compare in Figure S5 the spectral profile of the extinction $Q_{Ext}(\lambda_L)$ of such a dimer and that of the local field intensity enhancement factor (LFIEF) $M_{Loc}(\lambda_L)$ in the gap (where it is maximum). As can be seen in Figure S6, at least close to the interaction plasmon resonance (at 520 nm), $M_{Loc}(\lambda_L)$ and $Q_{Ext}(\lambda_L)$ correlate very closely (up to a proportionality factor). It should be noted that when comparing different systems, the actual value of the extinction coefficient may not be correlated with the magnitude of the LFIEF[9], but for a given system, the wavelength dependence of the extinction coefficient usually provides a good approximation to the spectral profile of $M_{Loc}(\lambda_L)$. This approximation has in fact been used in the past in similar contexts[11-13].
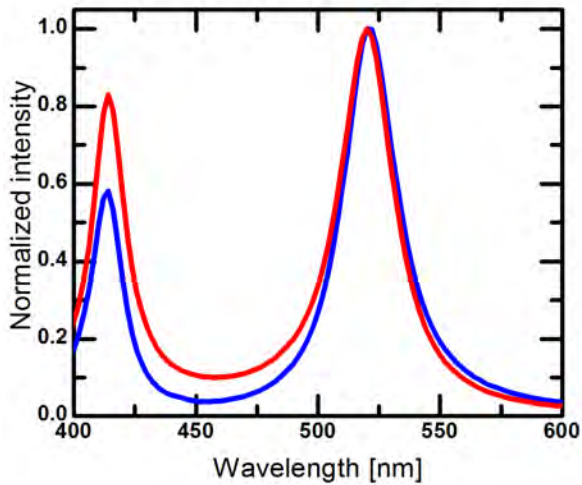

Figure S5: Normalized extinction (blue), and normalized field enhancement (red) spectra for the case of a dimer of 34 nm diameter silver particles with 1.5 nm gap embedded in water.

We now focus on the spectral dependence of the surface-enhanced fluorescence enhancement factor, $M_{\text{SEF}}(\lambda_{\text{L}}, \lambda_{\text{R}})$ for an emitter at a distance d from the metal surface. As explained in the main text, this factor can be approximated as:

$$M_{\text{SEF}} = M_{\text{Loc}}(\lambda_{\text{L}})\eta(\lambda_R)/Q_0 \tag{S1}$$

Where η is the modified quantum yield given by:

$$\eta(\lambda_R) = M_{Rad}(\lambda_R)/M_{\text{Tot}} \tag{S2}$$

M_{Tot} can moreover be decomposed into a radiative contribution, given by M_{Rad} and a non-radiative contribution M_{NR}. The latter can itself be decomposed into two distinct non-radiative contributions:

$$M_{NR} = M_{NR}^{LSP} + M_{NR}^{SPP} \tag{S3}$$

$M_{\text{NR}}^{\text{SPP}}$ represents coupling into non-radiative surface-plasmon polariton waves of the metal surface. This contribution is strongly distance-dependent and does not depend much on the geometry. In fact, it is well approximated[8,14-16] by the case of an emitter on a flat metal surface for which:

$$M_{NR} \approx \frac{3}{8(k_M d)^3} \text{Im}\left(\frac{\varepsilon - \varepsilon_M}{\varepsilon + \varepsilon_M}\right) \tag{S4}$$

where ε (ε_{M}) is the dielectric function of the metal (embedding medium), k_M is the wavevector in the embedding medium, and d is the distance to the surface. The expression above applies to a dipole perpendicular to the surface (a factor ½ should be added for a parallel dipole). Also, for very small distances, $d<1$ nm, non-local effects are expected to become important, and the above expression underestimates the real non-radiative rates. In any case, as illustrated in Figure S7, this factor varies dramatically with the distance, owing to the $1/d^3$ dependence, but not much with wavelength.

The second non-radiative contribution, M_{NR}^{LSP}, relates to coupling to the (mostly radiative) localized surface Plasmon resonance, which also contributes to M_{Rad}. As a result, M_{NR}^{LSP} is of the same order as M_{Rad}, and follows the same resonance profile and is not very distance-dependent.

Given this, we can identify two limiting cases for the modified quantum yield:

- SPP-dominated regime, i.e. when $M_{\mathrm{NR}}^{\mathrm{SPP}}$ dominates over M_{NR}^{LSP}. This regime will apply for the shortest distances. In this case, $M_{\mathrm{Tot}} \approx M_{\mathrm{NR}}^{\mathrm{SPP}}$ and has only a mild wavelength dependence in the region of the LSP resonance. As a result, the spectral profile of $\eta(\lambda_{\mathrm{R}})$ is governed by the factor $M_{\mathrm{Rad}}(\lambda_{\mathrm{R}})$ and is also typically much smaller than 1.

- LSP-resonance-dominated regime, i.e. when M_{NR}^{LSP} dominates over $M_{\mathrm{NR}}^{\mathrm{SPP}}$. This regime will apply for the largest distances. In this case, $M_{\mathrm{Tot}} \approx M_{\mathrm{NR}}^{LSP} + M_{\mathrm{Rad}}$ and follows the same resonance profile as $M_{\mathrm{Rad}}(\lambda_{\mathrm{R}})$. This resonant wavelength-dependence therefore cancels out in the ratio to obtain $\eta(\lambda_{\mathrm{R}})$, which therefore has only a mild wavelength dependence in the region of the LSP resonance ($\eta \approx 0.4$ in the example of Figure S6).

The distance from the surface, d, is the primary factor influencing which of these two regimes applies. The cross-over from one regime to the other occurs when $M_{\mathrm{NR}}^{\mathrm{SPP}} \approx M_{\mathrm{Rad}}$ and will therefore occur at shorter distances when local field enhancements (and therefore M_{Rad}) are large.

These ideas are further illustrated in the theoretical calculations summarized in Figure S6, using parameters relevant to the experiments presented in the main paper. In order to be able to vary the distance from the surface, we consider emitters on a line angled at $\alpha \approx 21^{\circ}$ from the dimer axis as shown in Figure S6(a). The maximum distance from the surface is therefore d=2 nm (in the 1.5 nm gap exactly between the spheres, the maximum distance is only 0.75 nm). As shown in Figure S6(a), the factor $M_{\mathrm{Rad}}(\lambda_{\mathrm{R}})$ exhibit a resonance associated with the localized Plasmon resonance of the dimer, but its magnitude is not strongly dependent on distance over the small range investigated here. In contrast, $M_{\mathrm{NR}}^{\mathrm{SPP}}$ is not very wavelength dependent but varies over several orders of magnitude as d changes (see Figure S6(b)). In the greyed area (short distances), it entirely dominates M_{Tot} as shown explicitly in Figure S6(c). As a result, the modified quantum yield $\eta(\lambda_{\mathrm{R}})$ follows closely the spectral profile of $M_{\mathrm{Rad}}(\lambda_{\mathrm{R}})$ in this regime (short distances). For larger distance, however, $\eta(\lambda_{\mathrm{R}})$ is of the order of 0.4 around the resonance and exhibit a much less pronounced wavelength dependence (Figure S6(d)).
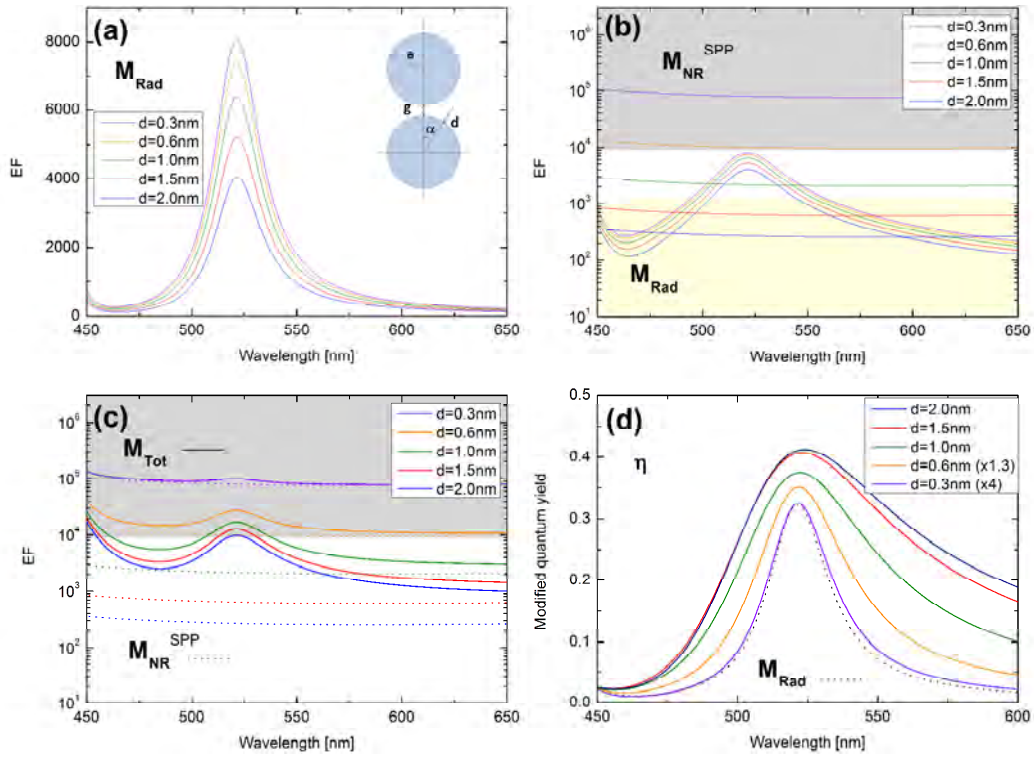
Figure S6: The influence of distance on the spectral profile and magnitude of the enhancement factors influencing the modified quantum yield in SEF conditions. All quantities are obtained from generalized Mie theory calculations on a dimer of silver spheres, with a dipole perpendicular to the surface positioned at a distance d from the surface along a line angled at $\alpha \approx 21^\circ$ from the dimer axis, as shown in the schematics in (a). We show in particular:

(a) the radiative enhancement factor M_{Rad}. (b) the SPP contribution to the non-radiative enhancement factor, M_{NR}^{SPP} (Eq. S4), also compared to M_{Rad}. Depending on their relative contributions, two regimes can be identified for the total decay rate enhancement M_{Tot}: SPP-dominated (greyed area) at short distances, and LSP-dominated (yellow area) at larger distances. This is also evident when comparing the predicted M_{Tot} and M_{NR}^{SPP} as shown in (c). The resulting modified quantum yield, $\eta = M_{Rad}/M_{Tot}$ is shown in (d). Its spectral profile is the same as that of M_{Rad} in the SPP-dominated regime (small d), but is much less pronounced around the resonance (0.4) in the LSP-dominated regime (larger d).

References:

(1)   Gill, R.; Le Ru, E. C. *Phys. Chem. Chem. Phys.* **2011**, *13*, 16366-16372.
(2)   Li, M.; Johnson, S.; Guo, H.; Dujardin, E.; Mann, S. *Adv. Funct. Mater.* **2011**, *21*, 851-859.
(3)   Stokkum, I. H. M.; Oort, B.; Mourik, F.; Gobets, B.; Amerongen, H. In *Biophysical Techniques in Photosynthesis*; Aartsma, T. J., Matysik, J., Eds.; Springer Netherlands: 2008; Vol. 26, p 223-240.
(4)   Rojas, R.; Claro, F. *J. Chem. Phys.* **1993**, *98*, 998-1006.
(5)   Gérardy, J. M.; Ausloos, M. *Phys. Rev. B* **1982**, *25*, 4204-4229.
(6)   Johansson, P.; Xu, H.; Käll, M. *Phys. Rev. B* **2005**, *72*, 035427.
(7)   Le Ru, E. C.; Etchegoin, P. G.; Meyer, M. *J. Chem. Phys.* **2006**, *125*, 204701.
(8)   Le Ru, E. C.; Etchegoin, P. G.; Grand, J.; Félidj, N.; Aubard, J.; Lévi, G. *J. Phys. Chem. C* **2007**, *111*, 16076-16079.
(9)   Le Ru, E. C.; Galloway, C.; Etchegoin, P. G. *Phys. Chem. Chem. Phys.* **2006**, *8*, 3083-3087.
(10)   Le Ru, E. C.; Meyer, M.; Blackie, E.; Etchegoin, P. G. *J. Raman Spectrosc.* **2008**, *39*, 1127-1134.
(11)   Le Ru, E. C.; Blackie, E.; Meyer, M.; Etchegoin, P. G. *J. Phys. Chem. C* **2007**, *111*, 13794-13803.
(12)   Le Ru, E. C.; Etchegoin, P. G.; Grand, J.; Félidj, N.; Aubard, J.; Lévi, G.; Hohenau, A.; Krenn, J. R. *Curr. Appl. Phys.* **2008**, *8*, 467-470.
(13)   Le Ru, E. C.; Grand, J.; Félidj, N.; Aubard, J.; Lévi, G.; Hohenau, A.; Krenn, J. R.; Blackie, E.; Etchegoin, P. G. *J. Phys. Chem. C* **2008**, *112*, 8117-8121.
(14)   Bharadwaj, P.; Novotny, L. *Opt. Express* **2007**, *15*, 14266-14274.
(15)   Novotny, L.; Hecht, B.; Cambridge University Press: 2006.
(16)   Le Ru, E. C.; Etchegoin, P. G. *Principles of surface enhanced Raman spectroscopy and related plasmonic effects*; Elsevier: Amsterdam, 2009.